Scientific Reports

https://doi.org/10.1038/s41598-026-56995-4

Article in Press

Radiomics-based fundus autofluorescence analysis in central serous chorioretinopathy–MICRoN report number twelve

Received: 4 March 2026

Accepted: 4 June 2026

Published online: 10 June 2026

Cite this article as: Sadeghi E., Peng L., Lall S.R. *et al.* Radiomics-based fundus autofluorescence analysis in central serous chorioretinopathy–MICRoN report number twelve. *Sci Rep* (2026). https://doi.org/10.1038/s41598-026-56995-4

Elham Sadeghi, Lingyi Peng, Shreyaa Rohindra Lall, Nasiq Hasan, Ryan Chace Williamson, Peranut Chotcomwongse, Paisan Ruamviboonsuk, Marco Lupidi, Marion R. Munk, Min Kim, Michael Zhang, Charles C. Wykoff, Gabriele Piccoli, Stela Vujosevic, Lihteh Wu, Yan Ma & Jay Chhablani

Radiomics-Based Fundus Autofluorescence Analysis in Central Serous Chorioretinopathy–MICRoN Report Number Twelve

Elham Sadeghi [1]; Lingyi Peng [2]; Shreyaa Rohindra Lall [1]; Nasiq Hasan [1]; Ryan Chace Williamson [1]; Peranut Chotcomwongse [3], Paisan Ruamviboonsuk [4], Marco Lupidi [5], Marion R. Munk [6-8], Min Kim [9], Michael Zhang [10-11], Charles C. Wykoff [12], Gabriele Piccoli [13]; Stela Vujosevic [13-14]; Lihteh Wu [15]; Yan Ma [2]; Jay Chhablani [1]

[1] Department of Ophthalmology, University of Pittsburgh, School of Medicine, Pittsburgh, PA, US

[2] Department of Biostatistics and Health Data Science, University of Pittsburgh

[3] Vitreoretina Unit, Department of Ophthalmology, Rajavithi Hospital, Rungsit University, Bangkok, Thailand

[4] Department of Ophthalmology, Rangsit University TH, Bangkok, Thailand

[5] Department of Experimental and Clinical Medicine, Eye Clinic, Polytechnic University of Marche, Ancona, Italy

[6] Gutblick, Pfäffikon, Switzerland

[7] Inselspital, University Hospital Bern, Bern, Switzerland

[8] Department of Ophthalmology, Northwestern University Feinberg School of Medicine, Chicago, IL, USA

[9] Department of Ophthalmology, Institute of Vision Research, Gangnam Severance Hospital

[10] The Canberra Hospital, Yamba Dr, Garran ACT 2605, Australia

[11] Sydney and Sydney Eye Hospital, 8 Macquarie St, Sydney NSW 200, Australia

[12] Retina Consultants of Texas, Retina Consultants of America, Blanton Eye Institute, Houston

[13] Eye Clinic, IRCCS MultiMedica, Milan, Italy.

[14] Department of Biomedical, Surgical and Dental Science University of Milan, Milan, Italy

[15] Asociados de Macula Vitreo y Retina de Costa Rica, San José, Costa Rica

Corresponding author

Jay Chhablani MD

UPMC Vision Institute

1622 Locust Street

Pittsburgh, PA 15219

jay.chhablani@gmail.com

Authors' email:

Elham Sadeghi: el.sadeghi91@gmail.com

Lingyi Peng: lingyi.peng@pitt.edu

Shreyaa Rohindra Lall: shreyaalall@gmail.com

Nasiq Hasan: nasiqimtiaz@gmail.com

Ryan Chace Williamson: williamsonr@upmc.edu

Peranut Chotcomwongse: peranut.chot@gmail.com

Paisan Ruamviboonsuk: paisan.trs@gmail.com

Marco Lupidi: dr.marco.lupidi@gmail.com

Marion R. Munk: Marion_munk@hotmail.com

Min Kim: minkim76@gmail.com

Michael Zhang: mgzhang90@gmail.com

Charles Wykoff: charleswykoff@gmail.com

Gabriele Piccoli: gabriele.piccoli95@gmail.com

Stela Vujosevic: stela.vujosevic@unimi.it

Lihteh Wu: lihteh@gmail.com

Yan Ma: yanma@pitt.edu

Jay Chhablani: jay.chhablani@gmail.com

Postal address for all the authors: 1622 Locust Street, Pittsburgh, PA 15219

Keywords: Radiomics, central serous chorioretinopathy, Fundus autofluorescence

Running head (short title): FAF radiomics features in CSCR

Abstract

This study applies radiomics-based feature extraction to fundus autofluorescence (FAF) images to automatically identify quantitative biomarkers that distinguish simple versus complex and acute versus chronic subtypes of central serous chorioretinopathy (CSCR). A total of 96 FAF images representing different CSCR stages were analyzed: simple (n=47), complex (n=49), acute (n=47), and chronic (n=49). Fifty-two radiomic features were extracted from the entire 55° FAF images using Pyfeats. Variables with zero variance and highly correlated features (Pearson's $r > 0.8$) were excluded. The most informative features were identified and used to construct and evaluate logistic regression, random forest, and extreme gradient boosting (XGBoost) classifiers for CSCR stage prediction. For simple versus complex CSCR, eight selected features yielded excellent discriminative performance in the logistic regression model, with a mean area under the receiver operating characteristic curve (AUC) of 0.90 (95% CI, 0.71–1.00) and an accuracy of 0.80. Sensitivity and specificity were balanced at 0.80 each, indicating robust and stable classification performance. For acute versus chronic CSCR, ten features were selected. The XGBoost model demonstrated modest discriminative ability with a mean AUC of 0.69 (95% CI, 0.39–0.98) and an accuracy of 0.71, with balanced sensitivity (0.70) and specificity (0.71) across resamples. Radiomic features extracted from FAF images effectively distinguish simple and complex CSCR, supporting their potential as quantitative imaging biomarkers for automated CSCR classification and disease staging.

Introduction

Central serous chorioretinopathy (CSCR) is a common macular disorder characterized by focal detachments of the neurosensory retina and/or the retinal pigment epithelium (RPE), and may affect one or both eyes. [1] Multimodal imaging, including fluorescein angiography, indocyanine green angiography, fundus autofluorescence (FAF), and optical coherence tomography (OCT), plays a central role in the diagnosis and classification of CSCR. [2] CSCR is commonly categorized as acute or chronic based on the duration of serous retinal detachment (SRD); eyes with SRD persisting for more than 3 to 6 months are considered to have chronic CSCR. [3] Although acute CSCR resolves spontaneously within 3 to 6 months in

most patients (78%–84%), recurrent active episodes occur in up to 50% of cases, contributing to cumulative damage and variable clinical outcomes. [3-6]

FAF imaging is a rapid, noninvasive technique that topographically maps the metabolic activity of fluorophores without requiring any intravenously injected agents. [7] It is particularly valuable for identifying RPE alterations and assessing the extent of disease burden. [8] Based on the area of RPE damage observed on FAF, CSCR can be classified as simple, defined as involving <2 disc diameters of RPE abnormality, or complex, defined as involving ≥2 disc diameters. [8]

Radiomics-based texture analysis applies standardized image-processing algorithms to extract quantitative texture features from medical images and has been widely implemented in radiology and pathology for diagnostic and prognostic modeling. [9,10] In recent years, its application within ophthalmology has expanded across multiple imaging modalities, including OCT, OCT angiography, fundus photography, and fluorescein angiography, to facilitate the prediction, classification, and monitoring of various retinal pathologies, such as CSCR, diabetic retinopathy, epiretinal membrane, age-related macular degeneration, optic neuropathies, and myopic maculopathy. [11-18] However, most prior studies have primarily focused on retinal layer analysis in OCT-based radiomics, with comparatively limited exploration of FAF imaging, despite its established role in CSCR follow-up, particularly for assessing RPE damage secondary to subretinal fluid (SRF) accumulation.

In this study, we apply radiomics feature extraction to FAF in patients with CSCR in different stages, including acute/chronic and simple/complex, to identify texture-based biomarkers associated with CSCR. We first ranked feature importance to identify the most informative features. Selected features were then evaluated in different classifier models to find the most accurate model that can predict acute vs. chronic, and simple vs. complex CSCR.

Results

Following exclusion of patients with incomplete data, the final cohort comprised 96 FAF images from 96 patients diagnosed with CSCR. The mean age of the participants was 48.28 ± 9.71 years. Of these, 24 patients (25%) were female, and 72 (75%) were male. Sixty-one eyes (63.5%) were right eyes, and 35 eyes (36.5%) were left eyes. Forty-seven cases

(48.9%) were classified as simple CSCR, and 49 (51.1%) as complex CSCR. Additionally, 47 cases (48.9%) were acute CSCR, whereas 49 (51.1%) were chronic CSCR.

Feature Selection and Model Performance for Predicting Simple vs. Complex CSCR

The ROCs of the three ML models in the testing cohort are shown in Fig 1. Among the three ML models, we found that logistic regression achieved the highest overall performance. The logistic regression model discrimination and stability evaluation demonstrated an excellent discriminative ability, with a mean area under the ROC curve (AUC) of 0.90 (95% CI 0.71–1.00) and strong overall accuracy of 0.80. Sensitivity and specificity were balanced at 0.80 and 0.80, respectively, indicating robust and consistent performance across resamples. (**Table 1 and 2, Figures 1-3**)

Feature Selection and Model Performance for Predicting Acute vs. Chronic CSCR

The ROC curves of the three machine learning models in the testing cohort are shown in **Figure 4**. Among the three models, XGBoost achieved the highest overall performance for differentiating acute versus chronic CSCR. The XGBoost model showed modest discriminative ability, with a mean AUC of 0.69 (95% CI, 0.39–0.98) and an accuracy of 0.71. Sensitivity and specificity were 0.70 and 0.71, respectively. Given the wide confidence interval, these findings should be interpreted cautiously. Feature importance for the random forest model is shown in Figure 5. (**Table 1**, **Figures 4 and 5**)

Discussion

We applied radiomics-based feature extraction on FAF images to identify quantitative biomarkers that distinguish simple versus complex and acute versus chronic subtypes of CSCR. For simple versus complex CSCR, eight selected features demonstrated excellent discriminative performance in the logistic regression model, yielding a mean AUC of 0.90 (95% CI, 0.71–1.00) and an accuracy of 0.80. Sensitivity and specificity were both 0.80. For acute versus chronic CSCR, ten features were selected, and XGBoost showed the highest performance among the tested models. However, its discriminative ability was only modest, with a mean AUC of 0.69 (95% CI, 0.39–0.98) and an accuracy of 0.71. Given the wide confidence interval, these results should be interpreted cautiously and suggest that FAF radiomics alone may have limited ability to distinguish acute from chronic CSCR.

CSCR is characterized by SRF resulting from choroidal vascular hyperpermeability and RPE dysfunction. Although most cases resolve spontaneously, a subset progresses to recurrent or chronic disease, leading to areas of hyper- or hypo-autofluorescence on FAF secondary to RPE damage. [19] CSCR is commonly categorized as acute versus chronic based on the duration of disease activity, or simple versus complex according to the extent of RPE involvement. [8] Previous research on the application of artificial intelligence in CSCR has explored several key domains of automated image analysis. [20] These include SRF segmentation [21-23], leakage point detection [23], choroidal and retinal vessel segmentation [24-29], segmentation of neurosensory retinal detachment, pigment epithelial detachment, and hyperreflective foci [30-33], as well as predictive modeling for CSCR recurrence and prognosis. [34-36]

In this study, radiomics features extracted from FAF images were associated with distinct CSCR phenotypes. These features reflect differences in autofluorescence intensity distribution and textural heterogeneity related to RPE dysfunction and disease chronicity. While clinicians can qualitatively recognize areas of hyper- or hypo-autofluorescence on FAF, radiomics enables objective quantification of subtle spatial patterns that are difficult to assess visually. From a clinical perspective, this approach may support more standardized phenotypic classification, improve longitudinal monitoring of RPE alterations over time, and provide an adjunctive tool for remote follow-up or telemedicine-based assessment where rapid, noninvasive imaging is desirable. The stronger performance observed for simple versus complex CSCR suggests that FAF radiomics may be particularly useful in identifying the extent of RPE involvement, which is clinically relevant for disease characterization and follow-up. In contrast, the relatively modest performance for acute versus chronic CSCR indicates that FAF-based texture features alone may be insufficient for this distinction, likely because chronicity is influenced by factors that are better captured through multimodal imaging and longitudinal clinical assessment. Therefore, FAF radiomics should currently be considered a complementary quantitative tool rather than a standalone method for clinical decision-making. Larger prospective studies integrating multimodal imaging will be important to determine its ultimate utility in patient management.

Unlike deep learning, radiomics-based feature extraction itself does not require model training, as predefined quantitative descriptors are directly computed from the images. However, when these extracted features are used for classification, the subsequent machine learning models still require training on labeled datasets. [15] Radiomics has been applied to

retinal diseases for diagnostic screening, predicting treatment response, differential diagnosis, staging, and monitoring. Most work focuses on AMD, diabetic retinopathy, CSCR, and other macular disorders, using OCT, OCTA, fundus photography, and ultra-widefield angiography to extract quantitative features that improve disease characterization. [12,15,16,18] Williamson et al. used radiomic feature extraction on OCT scans from patients with CSCR to identify biomarkers that distinguish healthy from diseased eyes. [15] In our study, we applied radiomic analysis to FAF images of CSCR patients and found that a logistic regression model achieved acceptable accuracy in differentiating simple from complex CSCR, offering potential value for patient follow-up and understanding disease progression over time.

The main limitations of this study include its cross-sectional, retrospective design, small sample size, and absence of wide-field imaging. Axial length data were unavailable and could not be analyzed, which may have influenced radiomic features and model performance. Also, all included images were acquired using a single imaging platform (Heidelberg Spectralis), and the applicability of these findings to other FAF devices remains uncertain. Images were also filtered for quality, and those with artifacts or poor image quality were excluded; therefore, model performance may be lower when applied to datasets with a broader range of image qualities. In addition, although the dataset was assembled from multiple centers and likely included participants from diverse racial and ethnic backgrounds, standardized race and ethnicity data were not consistently available and therefore could not be analyzed, which may limit assessment of model generalizability across specific populations. Larger longitudinal studies will be required to validate these findings and demonstrate their potential to support the development of clinical decision-making tools that improve patient management across diverse chorioretinal diseases.

Overall, our results show that radiomics texture analysis of FAF images can identify features distinguishing simple from complex CSCR, with logistic regression demonstrating promising classification performance. Although XGBoost showed the highest performance for differentiating acute and chronic CSCR, the discriminative ability was modest and associated with a wide confidence interval, indicating substantial uncertainty. Therefore, FAF radiomics alone may be insufficient for reliable acute-versus-chronic classification and should be interpreted as a complementary rather than standalone approach. These findings suggest that radiomics features capture meaningful RPE alterations in CSCR and may have potential utility for future disease characterization and follow-up.

Method

Data Acquisition

We conducted a retrospective study utilizing 55° FAF images acquired with the Heidelberg Spectralis system (Heidelberg Engineering, Heidelberg, Germany) to collect high-quality images from patients diagnosed with CSCR exhibiting RPE damage. Only one image per patient was included. All participants gave written informed consent. The patients did not receive any financial compensation for their participation. The patients were advised that the data collected was used for scientific purposes, and they gave their consent for publication. The study adhered to the tenets of the Declaration of Helsinki and received approval from the Institutional Review Board of the University of Pittsburgh. All methods were performed in accordance with the relevant guidelines and regulations.

A total of 178 FAF images were initially reviewed for eligibility. Images were screened by an expert ophthalmologist for device compatibility, imaging protocol consistency, and image quality prior to radiomic analysis. To maintain technical uniformity, 45 images acquired using devices other than the Heidelberg Spectralis system were excluded. An additional 15 images were excluded because of a different field of view than the required 55° acquisition setting. Eighteen images were excluded because of poor image quality or artifacts, including shadowing, motion blur, poor focus, or other factors considered likely to interfere with reliable radiomic feature extraction from the full image. In 4 images, the model was not able to extract LTE features. Following this process, 96 FAF images from 96 patients were included in the final analysis.

Commonly, CSCR is further classified as acute or chronic based on the duration of neurosensory detachment, which persists for more than 3 to 6 months and is considered indicative of chronic CSCR. [3] CSCR cases were broadly categorized into simple and complex subtypes, with a 2-disc–area diameter of RPE atrophy defined as the threshold for classification. [8] A total of 96 FAF images were included in the following quality assessment, comprising 47 simple (48.9%) and 49 complex (51.1%) CSCR cases. Among these, 47 cases (48.9%) were categorized as acute CSCR, whereas 49 cases (51.1%) were chronic CSCR. All classifications were performed through clinical examination and evaluation of available multimodal imaging by expert retina surgeons. (**Figure 6**)

Exclusion criteria were applied to omit eyes with concomitant vitreoretinal pathologies, including age-related macular degeneration (AMD), uveitis, retinal vascular occlusion, and epiretinal membrane. Eyes with refractive error greater than ±2.5 diopters were also excluded. Eyes with other conditions that could compromise image quality, such as vitreous opacities or vitreous detachment, were also excluded. Images exhibiting artifacts, motion blur, or shadowing that could interfere with image acquisition or texture analysis were also excluded. Using the same device minimizes pixel-level variability between images. All included FAF images had uniform dimensions, an identical 55° field of view, and were confirmed to be of consistently high quality.

Feature Extractions

Radiomics feature extraction was performed on the entire 55° FAF images using Pyfeats, a Python-based radiomics library [37]. A total of 52 quantitative texture features were extracted from each image, encompassing four major categories: first-order statistics (FOS), gray-level co-occurrence matrix (GLCM), Gabor texture (GT), and Law's texture energy (LTE) [38-41]:

- FOS features (n = 16): quantified the intensity distribution of pixels, including percentiles (10th, 25th, 75th, and 90th), coefficient of variation, energy, entropy, histogram width, kurtosis, mean, median, mode, skewness, and variance. These features describe the global brightness and intensity variability across the image.
- GLCM features (n = 14): computed from co-occurrence matrices at a fixed pixel offset, including angular second moment, contrast, correlation, sum of squares variance, inverse difference moment, sum average, sum variance, sum entropy, entropy, difference variance, difference entropy, information measures of correlation, and maximal correlation coefficient. These parameters capture the spatial relationships and textural regularity between neighboring pixels.
- GT (Gabor) features (n = 16): obtained by normalizing pixel values to the range of −0.5 to 0.5 and applying Gabor filters with four orientations (0°, 45°, 90°, and 135°) and two spatial frequencies (0.1 and 0.4 cycles/pixel). The mean and standard deviation of the filtered outputs were computed for each orientation–frequency pair, representing multi-scale and multi-directional texture information.
- LTE features (n = 6): derived using Law's texture energy approach with a 3 × 3 convolution mask, capturing localized energy and directional texture patterns within the image.

Feature Selection for Machine Learning Analysis

We analysed a total of 55 initial variables, including 52 radiomics features and three patient-level variables (Age, Gender, and Right/Left eye). Four patients had missing measurements for all six LTE features. Given this missingness pattern, no imputation was performed; instead, a complete-case analysis was conducted, and these four patients were excluded from the study. To minimize redundancy, a pairwise collinearity analysis was performed using Pearson correlation coefficients. Variables exhibiting high collinearity ($r > 0.8$) were filtered, retaining only one representative variable from each correlated pair. Feature retention was based on overall interpretability, feature stability, and representation of the radiomic category, with preference given to variables more commonly used or more directly interpretable in prior radiomics literature. This filtering step was performed before model training and independently of outcome labels to reduce redundancy while avoiding information leakage. Following this selection process, 30 features were excluded, leaving 22 radiomics features for downstream modeling.

Construction of ML models and Performance Evaluation for Predicting Simple vs. Complex CSCR

The cohort was divided into training (80%) and testing (20%) sets using stratified random sampling. Three machine learning algorithms were trained: Logistic Regression (LR), Random Forest (RF), and Extreme Gradient Boosting (XGBoost).

For the Logistic Regression model, features were selected using the Least Absolute Shrinkage and Selection Operator (LASSO). This process identified nine key predictors: Age (years), FOS_Mean, FOS_Variance, FOS_Skewness, FOS_MaximalGrayLevel, GLCM_Contrast_Mean, GLCM_DifferenceEntropy_Mean, GT_th_0.0_freq_0.4_std, and LTE_SS_3. For the Random Forest and XGBoost models, embedded feature selection was performed automatically during training. Hyperparameters for these models were optimized via 5-fold cross-validation on the training data. Model performance was evaluated on the independent testing cohort. The primary metric was the Area Under the Receiver Operating Characteristic Curve (AUC). The mean AUC and 95% confidence intervals (CI) were calculated using image-level 1,000 bootstrap iterations. Additionally, accuracy, sensitivity, specificity, and precision were computed for each classifier.

Construction of ML Models and Performance Evaluation for Predicting Acute vs. Chronic CSCR

The same feature-selection and model-development process was applied to predict acute versus chronic CSCR using FAF images. For the logistic regression model, feature selection was performed using the Least Absolute Shrinkage and Selection Operator (LASSO), as described for the simple-versus-complex analysis. This process identified three predictors: FOS_Variance, FOS_MaximalGrayLevel, and GLCM_Contrast_Mean. Random Forest and XGBoost models were then constructed using the same training and evaluation protocol described above.

Software

All statistical analyses, including data splitting, feature selection, and model training, were implemented using Python (version 3.12.7).

Funding: Supported by NIH Core Grant P30 EY08098 to the Department of Ophthalmology, The Eye and Ear Foundation of Pittsburgh, and an unrestricted grant from Research to Prevent Blindness, New York, NY.

Financial disclosures: None.

Conflict of interest: No conflicting relationship exists with any author.

Ethics approval and consent to participate

All participants gave written informed consent. The study was approved by the local ethics committee. The patients did not receive any financial compensation for their participation. The patients were advised that the data collected was used for scientific purposes, and they gave their consent for publication.

Author's contribution:

E.S. & J.C.: contributed to study design, data gathering, manuscript writing, revision, and final approval.

R.W.: contributed to the radiomics model preparation.

S.L., N.H., P.C., P.R., M.L., M.M., M.K., M.Z., C.W., G.P., S.V., and L.W. contributed to data preparation, analyzing images, manuscript revision, and final approval.

L.P. and Y.M. contributed to statistical analysis, revision, and final approval.

Data availability: The datasets used and analyzed during the current study are available from the corresponding author upon reasonable request.

References

1 Daruich, A. *et al.* Central serous chorioretinopathy: recent findings and new physiopathology hypothesis. *Progress in retinal and eye research* **48**, 82-118 (2015).

2 Viggiano, P. *et al.* Pachychoroid disease spectrum: how multimodal imaging and OCT angiography have improved our knowledge. *Progress in Retinal and Eye Research*, 101372 (2025).

3 Daruich, A. *et al.* ACUTE CENTRAL SEROUS CHORIORETINOPATHY: Factors Influencing Episode Duration. *Retina* **37**, 1905-1915 (2017). https://doi.org:10.1097/iae.0000000000001443

4 Liew, G., Quin, G., Gillies, M. & Fraser-Bell, S. Central serous chorioretinopathy: a review of epidemiology and pathophysiology. *Clin Exp Ophthalmol* **41**, 201-214 (2013). https://doi.org:10.1111/j.1442-9071.2012.02848.x

5 Ozkaya, A., Alkin, Z., Ozveren, M., Yazici, A. T. & Taskapili, M. The time of resolution and the rate of recurrence in acute central serous chorioretinopathy following spontaneous resolution and low-fluence photodynamic therapy: a case-control study. *Eye (Lond)* **30**, 1005-1010 (2016). https://doi.org:10.1038/eye.2016.79

6 Loo, R. H. *et al.* Factors associated with reduced visual acuity during long-term follow-up of patients with idiopathic central serous chorioretinopathy. *Retina* **22**, 19-24 (2002).

7 Schmitz-Valckenberg, S. *et al.* Fundus autofluorescence imaging. *Progress in Retinal and Eye Research* **81**, 100893 (2021). https://doi.org:https://doi.org/10.1016/j.preteyeres.2020.100893

8 Chhablani, J. *et al.* Multimodal Imaging-Based Central Serous Chorioretinopathy Classification. *Ophthalmology Retina* **4**, 1043-1046 (2020). https://doi.org:10.1016/j.oret.2020.07.026

9 Coroller, T. P. *et al.* Radiomic phenotype features predict pathological response in non-small cell lung cancer. *Radiotherapy and oncology* **119**, 480-486 (2016).

10 Zhang, G. *et al.* CT-based radiomics to predict the pathological grade of bladder cancer. *European Radiology* **30**, 6749-6756 (2020).

11 Banerjee, I. *et al.* Prediction of age-related macular degeneration disease using a sequential deep learning approach on longitudinal SD-OCT imaging biomarkers. *Scientific Reports* **10**, 15434 (2020). https://doi.org:10.1038/s41598-020-72359-y

12 Carrera-Escalé, L. *et al.* Radiomics-based assessment of OCT angiography images for diabetic retinopathy diagnosis. *Ophthalmology Science* **3**, 100259 (2023).

13 Savastano, M. C. *et al.* Radiomic Feature Extraction from OCT Angiography of Idiopathic Epiretinal Membranes and Correlation with Visual Acuity: A Pilot Study. *Ophthalmology Science* **5**, 100716 (2025).

14 Meng, Z. *et al.* Machine learning and optical coherence tomography-derived radiomics analysis to predict persistent diabetic macular edema in patients

undergoing anti-VEGF intravitreal therapy. *Journal of Translational Medicine* **22**, 358 (2024).
15 Williamson, R. C. *et al.* Radiomics-Based OCT Analysis of Choroid Reveals Biomarkers of Central Serous Chorioretinopathy. *Translational Vision Science & Technology* **14**, 23-23 (2025).
16 Williamson, R. C. *et al.* Radiomics-based prediction of anti-VEGF treatment response in neovascular age-related macular degeneration with pigment epithelial detachment. *Translational Vision Science & Technology* **12**, 3-3 (2023).
17 Williamson, R. *et al.* Radiomics-based OCT analysis of unaffected fellow eyes uncovers biomarkers of central serous chorioretinopathy. *Investigative Ophthalmology & Visual Science* **66**, 1724-1724 (2025).
18 Zhang, H. *et al.* Radiomics in ophthalmology: a systematic review. *European Radiology* **35**, 542-557 (2025).
19 Sahoo, N. K. *et al.* Clinical and imaging characteristics of central serous chorioretinopathy with subfoveal leak. *European Journal of Ophthalmology* **0**, 11206721251378338 https://doi.org:10.1177/11206721251378338
20 Zhang, P., Zhang, Q., Hu, X., Chi, W. & Yang, W. Research Progress in Artificial Intelligence for Central Serous Chorioretinopathy: A Systematic Review. *Ophthalmology and Therapy* **14**, 2083-2107 (2025). https://doi.org:10.1007/s40123-025-01209-9
21 Yoo, T. K., Kim, B. Y., Jeong, H. K., Kim, H. K., Yang, D. & Ryu, I. H. Simple code implementation for deep learning–based segmentation to evaluate central serous chorioretinopathy in fundus photography. *Translational Vision Science & Technology* **11**, 22-22 (2022).
22 Xu, F. *et al.* Deep learning for detecting subretinal fluid and discerning macular status by fundus images in central serous chorioretinopathy. *Frontiers in Bioengineering and Biotechnology* **9**, 651340 (2021).
23 Wu, M. *et al.* Automatic subretinal fluid segmentation of retinal SD-OCT images with neurosensory retinal detachment guided by enface fundus imaging. *IEEE Transactions on Biomedical Engineering* **65**, 87-95 (2017).
24 Maruyama, K. *et al.* Diagnosis of choroidal disease with deep learning-based image enhancement and volumetric quantification of optical coherence tomography. *Translational Vision Science & Technology* **11**, 22-22 (2022).
25 Zhu, L. *et al.* Choroidal Optical Coherence Tomography Angiography: Noninvasive Choroidal Vessel Analysis via Deep Learning. *Health Data Science* **4**, 0170 (2024).
26 Liu, Y. *et al.* AI-based 3D analysis of retinal vasculature associated with retinal diseases using OCT angiography. *Biomedical Optics Express* **15**, 6416-6432 (2024).
27 Xu, J., Shen, J., Wan, C., Jiang, Q., Yan, Z. & Yang, W. A few-shot learning-based retinal vessel segmentation method for assisting in the central serous chorioretinopathy laser surgery. *Frontiers in Medicine* **9**, 821565 (2022).
28 Singh, S. R. *et al.* Three-dimensional choroidal vessels assessment in fellow eyes of patients with central serous chorioretinopathy. *Investigative Ophthalmology & Visual Science* **66**, 2781-2781 (2025).
29 Valsecchi, N. *et al.* Volumetric choroidal biomarkers in central serous chorioretinopathy using swept-source optical coherence tomography: a deep learning approach. *Graefe's Archive for Clinical and Experimental Ophthalmology*, 1-10 (2025).

30 Xing, R., Niu, S., Gao, X., Liu, T., Fan, W. & Chen, Y. Weakly supervised serous retinal detachment segmentation in SD-OCT images by two-stage learning. *Biomedical Optics Express* **12**, 2312-2327 (2021).
31 Wu, M. *et al.* Three-dimensional continuous max flow optimization-based serous retinal detachment segmentation in SD-OCT for central serous chorioretinopathy. *Biomedical optics express* **8**, 4257-4274 (2017).
32 Xue, J. *et al.* Deep ensemble neural-like P systems for segmentation of central serous chorioretinopathy lesion. *Information Fusion* **65**, 84-94 (2021).
33 Wei, J., Yu, S., Du, Y., Liu, K., Xu, Y. & Xu, X. Automatic segmentation of hyperreflective foci in OCT images based on lightweight DBR network. *Journal of Digital Imaging* **36**, 1148-1157 (2023).
34 Seiler, E. *et al.* Importance of OCT-derived biomarkers for the recurrence of central serous chorioretinopathy using statistics and predictive modelling. *Scientific reports* **14**, 23940 (2024).
35 Arrigo, A. *et al.* Structural OCT parameters associated with treatment response and macular neovascularization onset in central serous chorioretinopathy. *Ophthalmology and therapy* **10**, 289-298 (2021).
36 Ra, H. *et al.* Prediction of short-term anatomic prognosis for central serous chorioretinopathy using a generative adversarial network. *Graefe's Archive for Clinical and Experimental Ophthalmology*, 1-9 (2025).
37 Giakoumoglou, N. PyFeats: open source software for image feature extraction. *GitHub repository* (2021).
38 Haralick, R. M., Shanmugam, K. & Dinstein, I. H. Textural features for image classification. *IEEE Transactions on systems, man, and cybernetics*, 610-621 (2007).
39 Laws, K. I. in *Image processing for missile guidance.* 376-381 (Spie).
40 D, G. Theory of communication. *J Institution Electrical Eng* **94**, 58-58 (1947).
41 Gabor, D. Theory of communication. Part 1: The analysis of information. *Journal of the Institution of Electrical Engineers-part III: radio and communication engineering* **93**, 429-441 (1946).

Figure 1. Receiver operating characteristic (ROC) curves for classification of simple versus complex CSCR using three machine learning models with five-fold cross-validation. Logistic regression achieved the highest discriminative performance (AUC = 0.90), followed by random forest (AUC = 0.86) and XGBoost (AUC = 0.80). The dashed diagonal line represents chance-level discrimination (AUC = 0.5).

Figure 2. Feature correlation heatmap of radiomic descriptors extracted from FAF images. The matrix displays Pearson correlation coefficients (r) among 52 radiomic features. Strong correlations ($|r| > 0.8$, shown in dark red) indicate redundancy among features, particularly within the Gabor texture (GT) and Law's texture energy (LTE) categories, with additional correlations observed among selected gray-level co-occurrence matrix (GLCM) features. These correlated features were removed prior to model training to reduce multicollinearity.

Figure 3. Odds ratios of selected features from the final logistic regression model for complex CSCR. Odds ratios (ORs) from the final logistic regression model are shown for each selected feature. Features shown in red have ORs greater than 1, indicating a positive association with complex CSCR, whereas features shown in blue have ORs less than 1, indicating a negative association. Features with ORs close to 1 should be interpreted as having minimal estimated effect. The length of each bar represents the magnitude of the estimated association.

Figure 4. Receiver operating characteristic (ROC) curves for classification of acute versus chronic CSCR using three machine learning models with five-fold cross-validation. XGBoost achieved the highest discriminative performance (AUC = 0.69), followed by logistic regression (AUC = 0.61) and random forest (AUC = 0.57). The dashed diagonal line represents chance-level discrimination (AUC = 0.5).

Figure 5. The top 15 most important features in the XGBoost classifier.

Feature importance ranking derived from the XGBoost classifier, indicating the relative contribution of each variable to model performance. Higher importance values represent greater influence on the model's classification of chronic CSCR. The most influential features included GT_th_0.0_freq_0.4_mean, GT_th_1.0_freq_0.1 std, and GT_th_3.0_freq_0.1_mean.

Figure 6. Fundus autofluorescence images in acute (A) vs. chronic (B), and simple (C) vs. complex (D) CSCR.

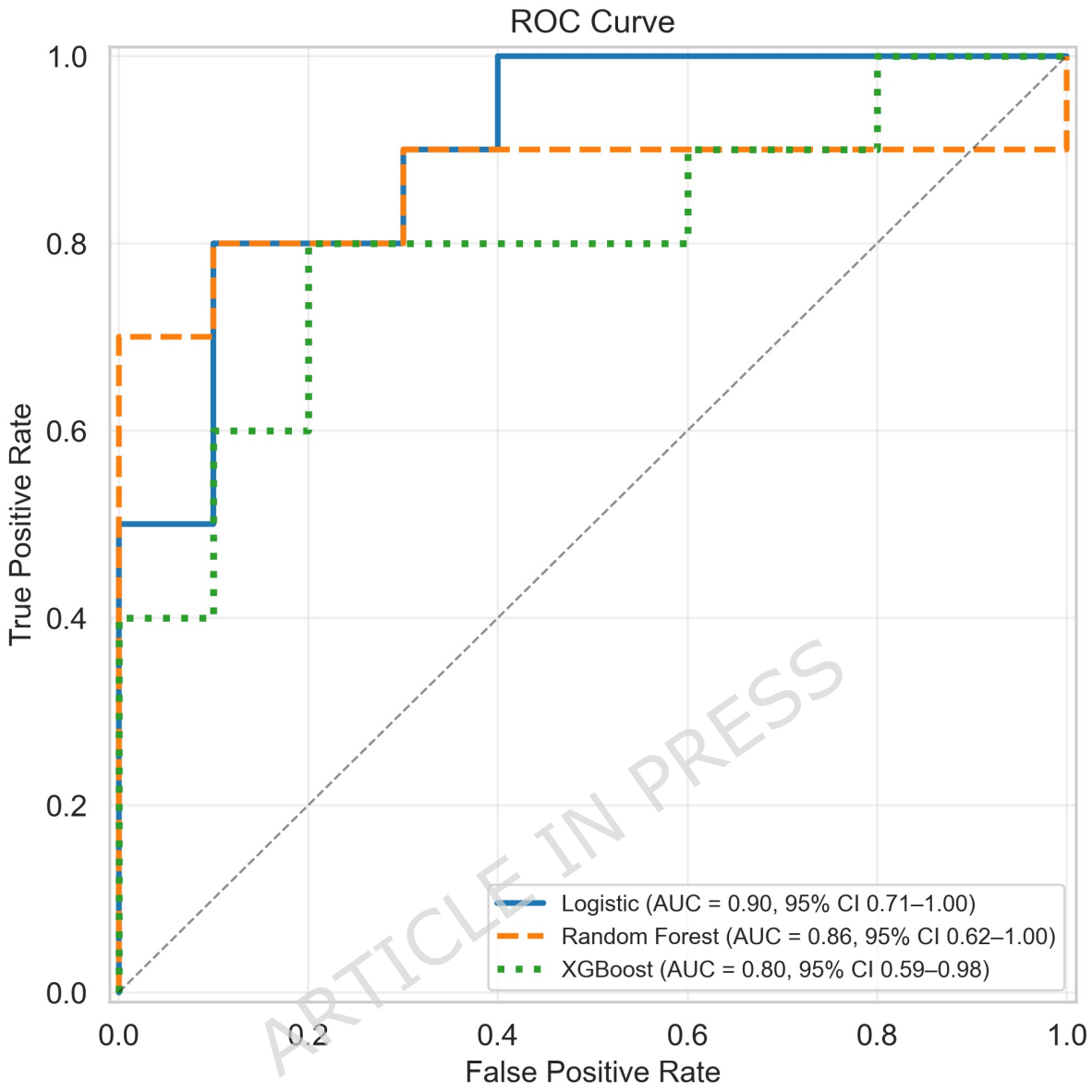

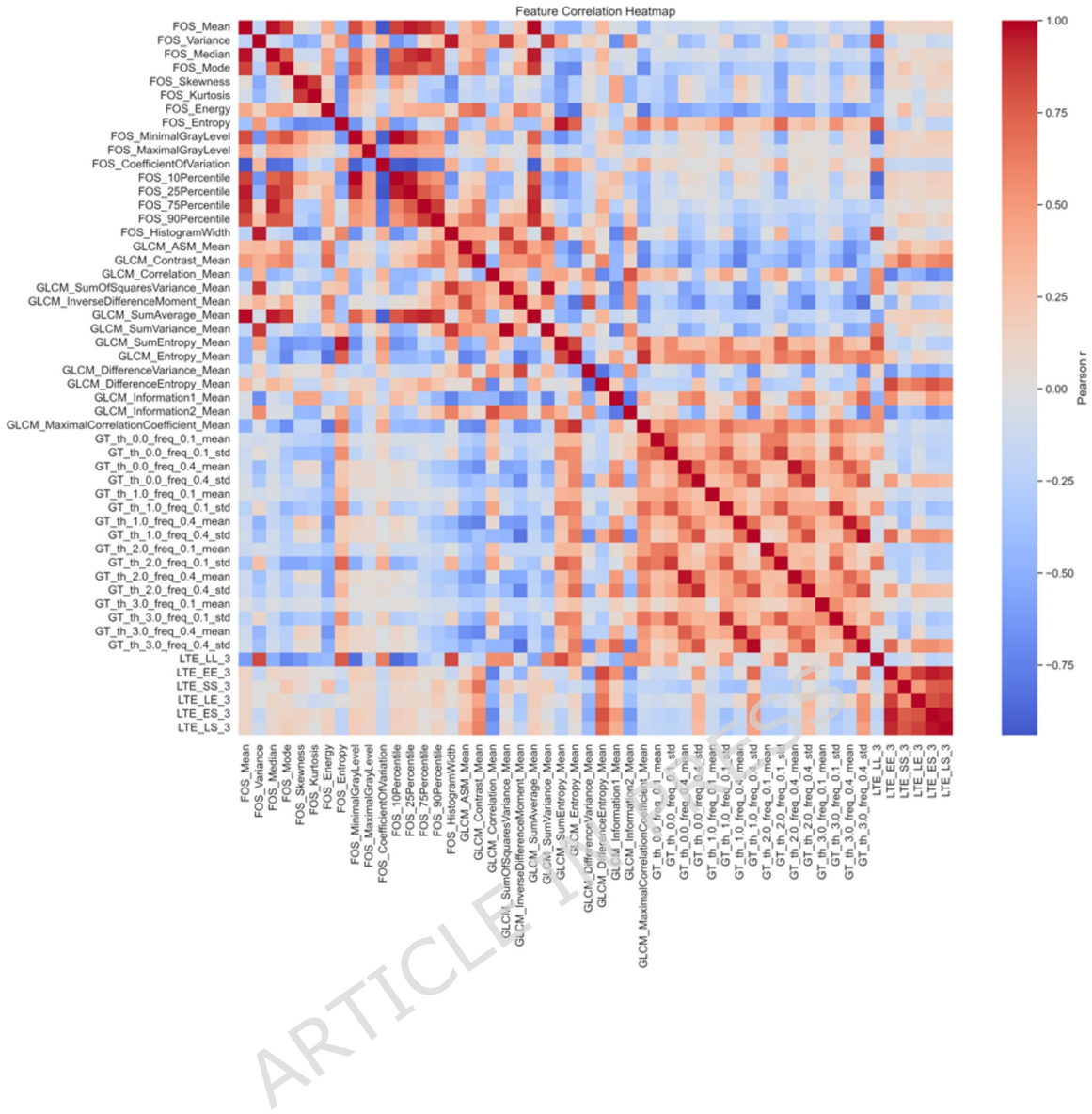

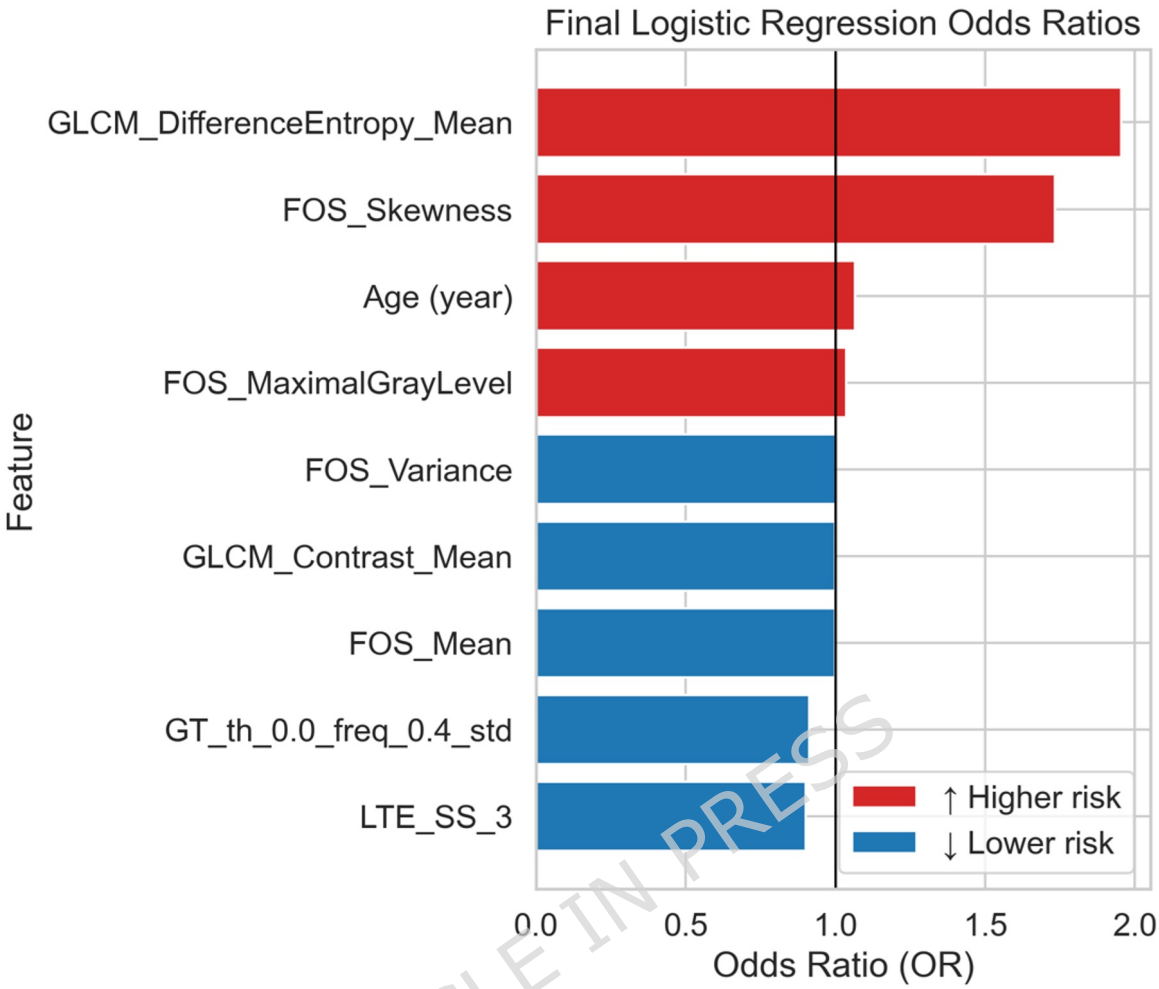

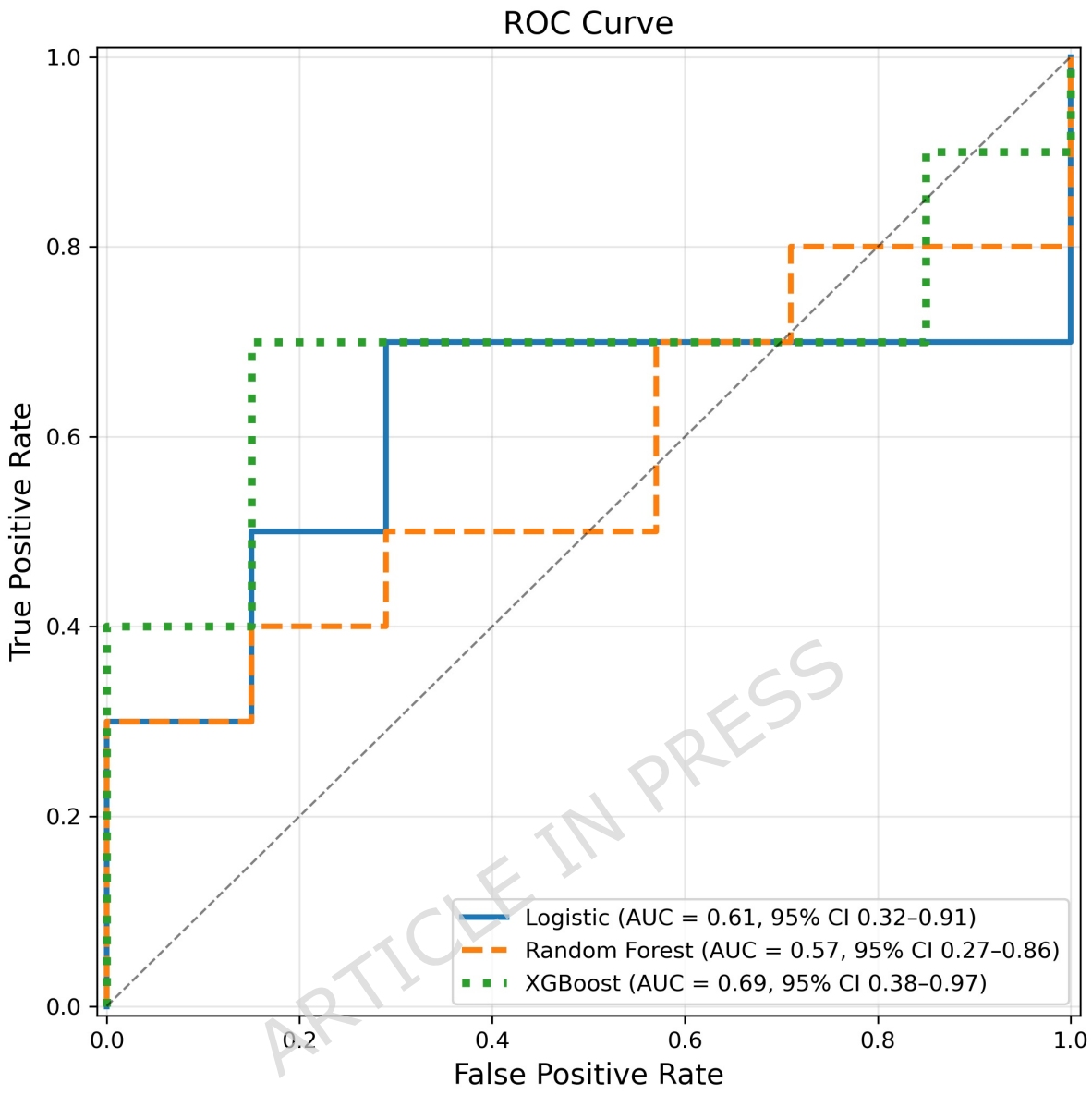

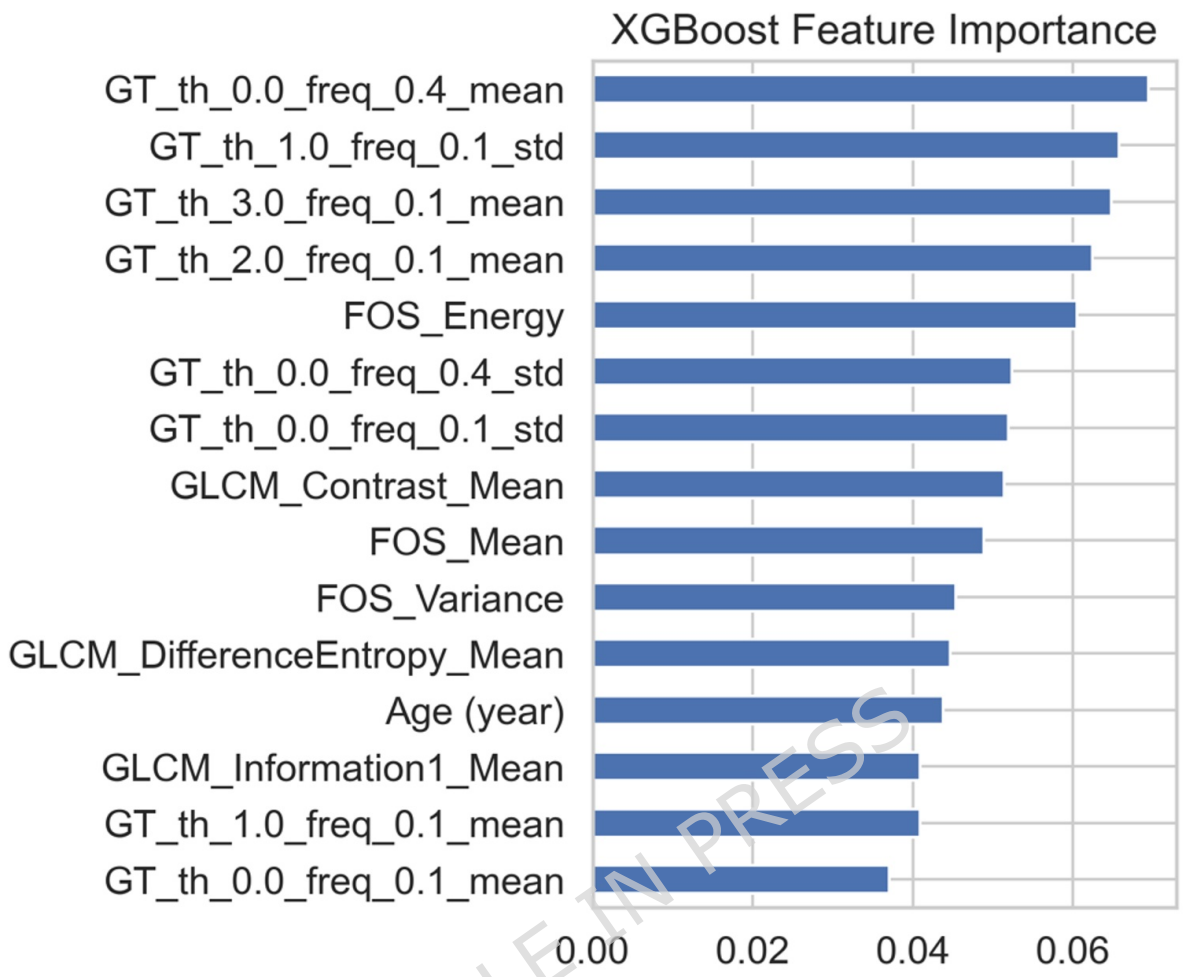

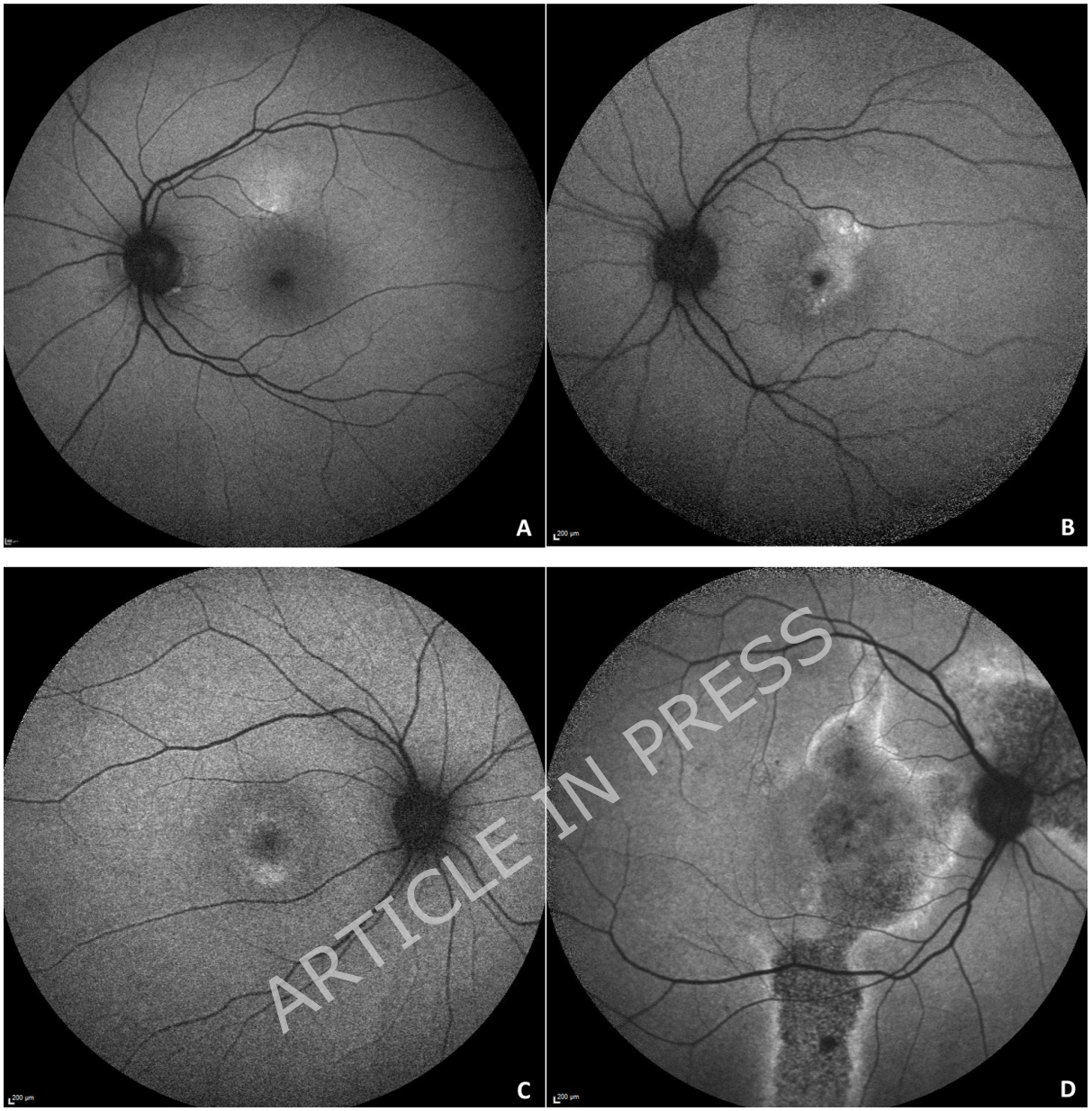

Model	ROC AUC (95% CI)	Accuracy	Sensitivity	Specificity	Precision
Logistic Regression	0.90 (0.71, 1.00)	0.80	0.80	0.80	0.80
Random Forest	0.86 (0.63, 1.00)	0.80	0.90	0.70	0.75
XGBoost	0.80 (0.59, 0.98)	0.70	0.80	0.60	0.67

Table 1-A: Simple vs. complex.

Classification performance of logistic regression, random forest, and XGBoost models for differentiating CSCR phenotypes based on fundus autofluorescence (FAF) radiomics features.

Logistic Regression	0.64 (0.32, 0.91)	0.59	0.30	1.00	1.00
Random Forest	0.57 (0.27, 0.86)	0.53	0.50	0.57	0.63
XGBoost	0.69 (0.39, 0.98)	0.71	0.70	0.71	0.78

Table 1-B: Acute vs. chronic.

Performance of radiomics-based machine learning models for classification of CSCR phenotypes using fundus autofluorescence (FAF) images.

Feature	Coefficient	Odds Ratio	Direction
GLCM_DifferenceEntropy_Mean	0.67001159	1.95425998	Higher risk
FOS_Skewness	0.54988139	1.73304744	Higher risk
LTE_SS_3	-0.1040824	0.90115108	Higher risk
GT_th_0.0_freq_0.4_std	-0.0914238	0.91263083	Higher risk
Age (year)	0.0625168	1.06451234	Higher risk
FOS_MaximalGrayLevel	0.03579153	1.03643976	Higher risk
FOS_Mean	-0.0016206	0.99838069	Lower risk
GLCM_Contrast_Mean	-0.0014048	0.99859623	Lower risk
FOS_Variance	-0.0002682	0.99973187	Lower risk

Table 2. Summary of logistic regression coefficients, odds ratios, and effect directions.

Table showing the coefficients, corresponding odds ratios, and direction of effect (higher or lower risk of being complex) for each selected feature in the final logistic regression model.